Biomacromolecules

Article

Cite This: Biomacromolecules 2019, 20, 3076−3086

pubs.acs.org/Biomac

gH625 Cell-Penetrating Peptide Promotes the Endosomal Escape of Nanovectorized siRNA in a Triple-Negative Breast Cancer Cell Line

Sanaa Ben Djemaa,[†] Katel Hervé-Aubert,[†] Laurie Lajoie,[‡,§] Annarita Falanga,[∥] Stefania Galdiero,[⊥] Steven Nedellec,[#] Martin Soucé,[†] Emilie Munnier,[†] Igor Chourpa,[†] Stéphanie David,[†] and Emilie Allard-Vannier*[,†]

[†]EA6295 Nanomédicaments et Nanosondes, University of Tours, 37200 Tours, France

[‡]EA7501 Groupe Innovation et Ciblage Cellulaire, Equipe Fc Récepteurs, Anticorps et MicroEnvironnement, University of Tours, 37032 Tours, France

[§]Plateforme Scientifique et Technique, Analyse des systèmes biologiques département des cytométries, University of Tours, 37032 Tours, France

[∥]Department of Agricultural Sciences, University of Naples "Federico II", Via Università 100, 80055 Portici, Italy

[⊥]Department of Pharmacy, CIRPEB—University of Naples "Federico II", Via Mezzocannone 16, 80134 Napoli, Italy

[#]Plateforme microPICell, SFR santé François Bonamy-IRSUN, 8 quai Moncousu, BP 70721, 44007 Nantes Cedex, France

Supporting Information

ABSTRACT: The use of small interfering RNA (siRNA) to regulate oncogenes appears as a promising strategy in the context of cancer therapy, especially if they are vectorized by a smart delivery system. In this study, we investigated the cellular trafficking of a siRNA nanovector (called CS-MSN) functionalized with the cell-penetrating peptide gH625 in a triple-negative breast cancer model. With complementary techniques, we showed that siRNA nanovectors were internalized by both clathrin- and caveolae-mediated endocytosis. The presence of gH625 at the surface of the siRNA nanovector did not modify the entry pathway of CS-MSN, but it increased the amount of siRNA found inside the cells. Results suggested an escape of siRNA from endosomes, which is enhanced by the presence of the peptide gH625, whereas nanoparticles continued their trafficking into lysosomes. The efficiency of CS-MSN to inhibit the GFP in MDA-MB-231 cells was 1.7-fold higher than that of the nanovectors without gH625.

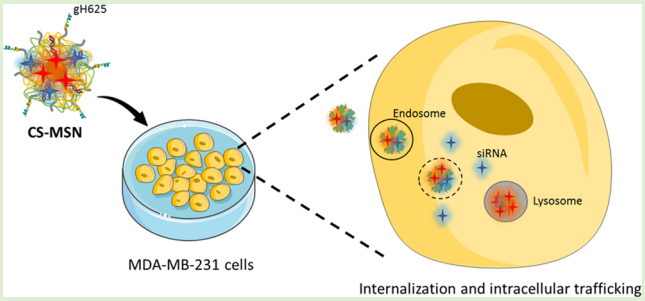

1. INTRODUCTION

The use of small interfering RNA (siRNA) for the treatment or the improvement of the treatment of serious diseases, such as cancer, has attracted great attention since the discovery of the RNA interference (RNAi) mechanism. This strategy is considered as a powerful alternative for noneffective therapies.[1] However, the use of these siRNA has some limitations related to their properties including the sensitivity to enzymatic degradation, difficulties to cross cell membranes, and accessibility to the cytoplasm.[2,3] Therefore, to overcome these difficulties, the development of an effective siRNA delivery tool is essential. One promising approach is the nanovectorization of siRNA, which consists of the complexation of siRNA with other components, leading to the formulation of nanosized complexes. Nanovectorization of siRNA is associated with some benefits such as (i) the protection of loaded siRNA from degradation in the biological environments, (ii) the gain of access and the accumulation in cells, and (iii) the increase of siRNA activity resulting from the siRNA half-life extension.[3]

To improve the siRNA nanovector efficacy, many research groups are interested to enhance cell internalization through the addition of surface ligands. The use of cell-penetrating peptides (CPP), also called membranotropic peptides, in siRNA nanovector development has recently received considerable attention, and it has shown promising results.[4−6] Indeed, CPP are a group of short positively charged peptides, able to cross the cell membrane bilayer both in an energy-dependent or -independent manner.[7] This property is well suitable for siRNA delivery systems to facilitate the passage of biological barriers. The CPP gH625 is a membrane-interacting domain of Herpes simplex virus type 1,[8] which has been shown to have a great ability to cross the cell membrane and

Received: May 8, 2019
Revised: July 10, 2019
Published: July 15, 2019

DOI: 10.1021/acs.biomac.9b00637
Biomacromolecules 2019, 20, 3076−3086

biological barriers and to successfully deliver different cargoes.[9−12] Associated with siRNA nanovectors, this peptide could be an addition or an alternative to targeting ligands, to enhance the efficiency in the treatment of some diseases when targeted cells do not overexpress any specific receptor or marker at their surface. A well-known model for such diseases is triple-negative breast cancer (TNBC). This cancer is defined by a lack of expression of the estrogen receptor, progesterone receptor, and human epidermal growth factor receptor 2 (HER2) by cancer cells,[13] which prevents the active targeting and favors the passive targeting by the enhanced permeability and retention (EPR) effect. The synergy between the EPR effect and the use of the CPP could offer an effective treatment for TNBC.

During the last decade, the siRNA nanovectors have made considerable progress in terms of developing formulation strategies and *in vitro* and *in vivo* assays. Numerous promising siRNA nanovectors have appeared with high downregulation efficiency of targeted genes.[14−16] Nevertheless, the internalization mechanisms and the intracellular trafficking of these siRNA nanovectors are poorly studied. Answering questions about the entry route of the nanovector, the release of siRNA inside the cells, the mechanisms of siRNA endosomal escape, and the monitoring of the components of the nanovector could provide more information about the improvement of the nanovector formulation and may explain the obtained efficiency of gene silencing.

We recently developed a siRNA nanovector based on fluorescent PEGylated superparamagnetic iron oxide nanoparticles (SPION) functionalized with the CPP gH625.[17] This nanoplatform was loaded, by electrostatic assembly, with siRNA and cationic polymers (chitosan and poly-L-arginine) to obtain CPP-capped stealth magnetic siRNA nanovectors called CS-MSN.[18] In the present study, we investigate the internalization and the intracellular trafficking of CS-MSN in the MDA-MB-231 TNBC cell line using their imaging properties thanks to their fluorescent labeling or their iron oxide core. In parallel, we highlighted the role of the peptide gH625 by comparing the trafficking and the monitoring of siRNA nanovectors with and without this CPP.

2. MATERIALS AND METHODS

2.1. Synthesis of gH625. The peptide gH625 with a cysteine at the C-terminal was synthesized by the standard Fmoc solid-phase method on a Rink amide resin. The amino acids were attached to the resin support; the first coupling was conducted in the presence of 4 equiv Fmoc-protected amino acid, 4 equiv DIC, and 4 equiv OxymaPure, whereas the second coupling was conducted in the presence of 4 equiv amino acid, 4 equiv HATU, and 8 equiv DIPEA. The crude peptide was cleaved with an acid solution of trifluoroacetic acid (TFA), precipitated with ice-cold diethyl ether, and purified by HPLC. The linear gradient used was 20−80% of acetonitrile in water (both containing 0.1%TFA) on a Phenomenex Jupiter 4 μm Proteo 90 Å 250 × 21.20 mm^2 column with UV detection at 210 nm. The pure peptide was analyzed by LC-MS.

2.2. Nanoparticle Preparation. The preparation of labeled and PEGylated superparamagnetic iron oxide nanoparticles (SPION) functionalized with the gH625 peptide is based on a previously published protocol,[17] with some modifications. Amino-silanized SPION were successively functionalized with sulfocyanine 5-NHS ester, NHS-PEG-maleimide, and the cell-penetrating peptide gH625. We substituted the hydrophobic cyanine 5,5-NHS by the hydrophilic sulfocyanine 5-NHS to facilitate purification. The resulting functionalized nanoparticles, further called CS-FNP (as CPP-capped stealth fluorescent nanoparticles), were purified by size-exclusion chromatography (SEC, detailed in Section 2.3.4). CS-FNP suspension was then concentrated by a Vivaspin concentrator with a cutoff of 30 kDa. A control batch of nanoparticles without gH625 peptide, further called S-FNP (as stealth fluorescent nanoparticles), was synthesized by replacing the CPP solution by PBS buffer.

2.3. Physicochemical Characterization of Nanoparticles and siRNA Nanovectors. *2.3.1. Size and ζ-Potential Analysis.* The hydrodynamic diameter (HD) and ζ-potential (ZP) of (C)S-FNP were measured in PBS 1× and $NaNO_3$ solution (0.01 M), respectively, at an iron concentration of 50 mg/L. For "CPP-capped" stealth magnetic siRNA nanovector [(C)S-MSN], the HD, the polydispersity index (PDI), and the ZP were obtained after dilution in $NaNO_3$ (0.01 M) to obtain a constant ionic strength. These measurements were performed using a Nanosizer apparatus (Zetasizer, Malvern Instrument) at 25 °C. The mean values of HD given were based on intensity. Measurements are presented as mean values ± SD.

2.3.2. Atomic Absorption Spectroscopy. Atomic absorption spectroscopy (AAS) was used to determine iron concentration on nanoparticle suspension. For that, (C)S-FNPs were digested by adding concentrated hydrochloric acid (6 M) for at least 2 h and then diluted with hydrochloric acid (0.12 M). Measurements were performed at 248 nm, and the concentrations of the samples were determined using a calibration curve (iron concentrations of 0.25, 0.5, 1, 2, and 5 mg/L).

2.3.3. High-Performance Liquid Chromatography (HPLC). Th Ultimate 3000 HPLC apparatus (Dionex, Voisins le Bretonneux, France) using a mixture of acetonitrile (HPLC gradient grade, Fisher Chemical, Loughborough, U.K.) with 0.1% TFA (Sigma-Aldrich Chemie GmbH, Steinheim, Germany) and an aqueous solution of TFA at 0.1% as a mobile phase at a flow rate of 1 mL/min. The gradient elution program was set up from 20 to 80% of acetonitrile in 20 min. The injected volume of peptide solutions or nanoparticle suspensions was fixed at 5 μL. A Kromasil C18 reversed-phase column (150 × 4.6 mm^2) was used for the analysis, and the temperature of the column was fixed at 25 °C. The peptide was detected with a fluorescence detector (RF-10AXL Shimadzu) after excitation of the tryptophan residue (excitation at 280 nm, emission at 350 nm). Results were acquired and analyzed using the software Chromeleon 7. The calibration curve was obtained from peak areas of gH625 peptide solutions in Milli-Q water at concentrations of 0.05, 0.1, 0.2, 0.3, and 0.5 g/L, using the chromatographic conditions described above.

2.3.4. Size-Exclusion Chromatography (SEC). The purification of nanoparticles by eliminating the free gH625 peptide was performed by size-exclusion chromatography using an ÄKTApurifier FPLC system equipped with a prepacked Superdex 200 pg column (600 × 16 mm^2) (GE Healthcare Bio-Science AB, Uppsala, Sweden) and a PBS 1× solution as the mobile phase (flow rate of 1 mL/min). The injected volume was 5 mL at an iron concentration of 0.4 g/L. The different components of the suspension were detected using a UV/vis detector at 280 nm. Purified fractions containing either nanoparticles or the free peptide were collected.

2.3.5. Fluorescence Spectroscopy. The presence of gH625 in CS-FNP suspension was checked at an iron concentration of 10 mg/L in DMSO/PBS (3:1, v/v) using an FS5 spectrofluorometer (Edinburgh Instruments, Livingston, U.K.). Fluorescence emission spectra were recorded in the range of 300−450 nm with excitation of the tryptophan residue of the peptide at 280 nm.

2.4. Formulation of siRNA Nanovectors. Cell-penetrating-peptide (CPP)-capped stealth magnetic siRNA nanovectors (CS-MSN) and stealth magnetic siRNA nanovectors (S-MSN) were prepared as described in our previous publication.[18] Briefly, CS-MSN and S-MSN were formulated by the electrostatic assembly of siRNA and cationic polymers with CS-FNP and with S-FNP, respectively. Cationic polymers were chitosan (Cs, MW 110−150 kDa; degree of acetylation: ≤40 mol %) and poly-L-arginine (PLR, MW 15−70 kDa) (Sigma-Aldrich Chimie GmbH, St. Quentin Fallavier, France). The content of (C)S-FNP was related to that of iron and was defined by the iron/siRNA w/w ratio (mass ratio, MR), and that of cationic polymers was defined by the molar ratio of the positive charges of

DOI: 10.1021/acs.biomac.9b00637
Biomacromolecules 2019, 20, 3076−3086

amine groups (NH_3^+, hereafter named N) of each polymer and the negative charges of siRNA's phosphate groups (PO_4^{3-}, hereafter named P) (N/P ratio). siRNA were first precomplexed with PLR at an N_{PLR}/P ratio of 2 and then added to the mix of CS-FNP_chitosan or S-FNP_chitosan prepared at an MR of 10 and an N_{CS}/P ratio of 30 to obtain CS-MSN or S-MSN, respectively.

2.5. Gel Retardation Assay and Heparin Decomplexation Assay. Agarose gel electrophoresis was used to verify the loading of siRNA in nanovectors. S-MSN and CS-MSN were prepared to deposit a siRNA concentration of 1.2 μM per well. Heparin solution (Sigma-Aldrich Chemie GmbH, Steinheim, Germany) was added at a final concentration of 3 mg/mL to release siRNA and control their integrity after formulation. Before the deposition of samples, a loading buffer (Agarose gel loading dye 6×, Fisher, Bioreagents, Illkirch, France) was added. An agarose gel (1% w/v) was prepared containing 0.01% (v/v) ethidium bromide to visualize free siRNA. The migration was conducted in a Tris−acetate−EDTA 1× buffer (Acros Organics, Geel, Belgium) for 15 min at 150 V. UV imaging was used to visualize free siRNA using the EvolutionCapt software on a Fusion-Solo.65.WL imager (Vilbert Lourmat, Marne-la-Vallée, France).

2.6. Cell Culture. Triple-negative breast cancer cells MDA-MB-231 (ECACC, Salisbury, U.K.) and MDA-MB-231 stably expressing GFP (MDA-MB-231/GFP) (Euromedex, Souffelweyersheim, France) were maintained in Dulbecco's modified Eagle's medium (Gibco, Life Technologies, Paisley, U.K.) supplemented with 10% fetal bovine serum (Eurobio, Les Ulis, France), nonessential amino acid 1× (HyClone Laboratories, Logan, Utah), and 1% penicillin/streptomycin (Gibco, Life Technologies, Paisley, U.K.) at 37 °C in a humid atmosphere containing 5% CO_2. The culture medium was changed every 48−72 h, and the cells were removed using trypsin/EDTA (0.05%) (Gibco, Life Technologies, Paisley, U.K.) at 80% confluency.

2.7. Nanovector Uptake. *2.7.1. Imaging Flow Cytometry (Amnis ImageStream^X Mark II).* MDA-MB-231 cells were seeded at 2×10^6 cells per well in a 6-well plate for 24 h. After cellular adhesion, cells were incubated with CS-MSN or S-MSN prepared with a nontargeted siRNA-Atto390 conjugate (Sigma-Aldrich, St. Quentin Fallavier, France) (50 nM siRNA) in an equal part of complete medium and Opti-MEM medium (Gibco, Life Technologies, Paisley, U.K.) (1:1 v/v), further named transfection medium, and maintained in normal cell culture conditions for 15 min, 30 min, 1 h, 2 h, 4 h, or 24 h. Next, cells were detached using trypsin−EDTA 0.05%, washed using HBSS 1× solution (HyClone Laboratories, Logan, Utah), and fixed using 4% paraformaldehyde solution (Electron Microscopy Sciences, Hatfield, U.K.) for 15 min at room temperature. In each experiment, 10 000 events for each sample were acquired using a 12-channel Amnis ImageStream^X Mark II (Amnis Corp., part of EMD Millipore, Seattle, WA) imaging flow cytometer equipped with the 405, 488, and 642 nm lasers. MDA-MB-231 images were captured with the Inspire imaging flow cytometry software at 60× magnification and extended depth-of-field (EDF) function. Single-stained samples of 500 cells were also illuminated by the 405 and 642 nm lasers with the brightfield (BF) and darkfield inactivated to perform color compensation controls. The spectral compensation matrix was applied to each of the files. Cells in the best focus were identified using Gradient RMS of the BF image. Single cells were then separated from debris and doublets using a plot of the aspect ratio vs the area of the BF image. The intracellular fluorescence intensity of siRNA-Atto390 (channel 7) and that of sulfocyanine 5 (channel 11) conjugated to CS-FNP or S-FNP were analyzed among double-positive cells using "erode mask" (Erode (M04, 3)) with IDEAS v6.2 software (Amnis-Merck).

2.7.2. Confocal Microscopy. MDA-MB-231 cells were seeded at 15 $\times 10^3$ cells per well in a poly-D-lysine-coated Ibidi 8-well plate and were allowed to adhere for 48 h. The cell culture medium was replaced by the transfection medium, and then CS-MSN or S-MSN prepared with the siRNA-Atto390 conjugate (50 nM siRNA) was added for 4 h. After that, cells were washed, incubated or not for additional 20 h, and then stained with Wheat germ agglutinin-Alexa Fluor 488 (WGA-AF488) (Invitrogen by Thermo Fisher Scientific, Life Technologies Corporation, Eugene). For the staining of the cell membrane with WGA-AF488 conjugate, the transfection medium was replaced with WGA-AF488 solution (1.25 μg/mL) for 10 min. Next, cells were washed with DPBS 1× (HyClone Laboratories, Logan, Utah) and fixed with 4% paraformaldehyde solution for 15 min. Finally, cells were washed and mounted with Fluoromount-G (Invitrogen by Thermo Fisher Scientific, San Diego, CA). Cells were visualized and imaged with a confocal microscope Nikon A1R using ×60/1.4 objective and NIS elements software. Images were acquired with a resolution of 0.21 μm/px and were constructed using ImageJ software.

2.8. CS-MSN Internalization Pathway Determination. *2.8.1. Chemical Inhibitors of Internalization Pathways.* MDA-MB-231 cells were seeded at 85×10^3 cells per well in a 12-well plate for 24 h. After cellular adhesion, cells were incubated with chemical inhibitors of known endocytic pathways for 1 h in serum free medium, then CS-MSN or S-MSN (50 nM siRNA) were added for 4 h. Dynasore (100 μM, EMD, Millipore Corp) was used to inhibit dynamin, which is implicated in the formation of vesicles of many endocytosis processes. The combination between sodium azide (Sigma-Aldrich, Steinheim, Germany) and 2-deoxy-D-glucose (Alfa Aesar, Thermo Fisher GmbH, Erlenbachweg, Germany) (50 mM for both) was used to inhibit the energy-dependent internalization. Chlorpromazine (10 μg/mL, Sigma Life Science, Sigma-Aldrich, St Louis) and pitstop 2 (30 μM, Sigma Life Science, Sigma-Aldrich, St Louis), were used to disrupt clathrin-mediated endocytosis. Methyl-β-cyclodextrin (MβCD) (2.5 mM, Sigma Life Science, Sigma-Aldrich, St Louis) and nystatin (50 μg/mL, Sigma Life Science, Sigma-Aldrich, St Louis) were used to block caveolae-mediated endocytosis. Dimethyl amiloride (DMA) (200 mM, Sigma Life Science, Sigma-Aldrich, St Louis) was used to inhibit the internalization of nanovectors mediated by macropinocytosis. After incubation, cells were detached and fixed with 4% paraformaldehyde solution for 15 min. Finally, intracellular sulfocyanine 5 fluorescence was measured using a flow cytometer (Gallios flow cytometer, Beckman Coulter) equipped with a 642 nm laser and acquired by Gallios software. Data were analyzed by FlowJo v10 software.

2.8.2. Transmission Electron Microscopy Imaging. MDA-MB-231 cells were cultured in cell culture tubes at a concentration of 2×10^6 cells per tube. Thereafter, cells were incubated with S-MSN or CS-MSN (750 nM siRNA, equivalent of 100 mg/L of iron) for 4 h in a humidified atmosphere with 5% CO_2 at 37 °C and under constant agitation using a Stuart SB2 tube rotator (Bibby Scientific Ltd, U.K.). Nontreated cells were used as a negative control. After incubation, cells were washed three times with DBPS 1×, then fixed with Trump's solution consisting of 0.1 M phosphate buffer and 4% paraformaldehyde (Sigma, Steinheim, Germany) and 1% glutaraldehyde (EMS, Hatfield, PA). Cells were postfixed with 2% osmium tetroxide (EMS, Hatfield, PA), dehydrated with a series of increasing ethanol solutions, and embedded in Epon resin (Sigma, Steinheim, Germany). Ultrathin sections (90 nm) were stained with 2% aqueous uranyl acetate and 1% lead citrate (Merck, Darmstadt, Germany). Images were acquired using a JEOL 1011 transmission electron microscope operating at 100 kV.

2.9. Intracellular Trafficking of S-MSN and CS-MSN. *2.9.1. Confocal Microscopy.* MDA-MB-231 cells were seeded at 15 $\times 10^3$ cells per well in a poly-D-lysine-coated Ibidi 8-well plate and were allowed to adhere for 48 h. The cell culture medium was replaced by the transfection medium, and then S-MSN or CS-MSN prepared with the siRNA-Atto390 conjugate (50 nM) siRNA were added for 4 h. After that, cells were washed, incubated or not for additional 20 h, and then stained with WGA-AF488, anti-EEA-1-Alexa Fluor 488 (Abcam, Cambridge, U.K.) or anti-Lamp1-Alexa Fluor 488 (eBiosciences, Thermo Fisher Scientific, San Diego, CA) antibodies. For the staining with antibodies, cells were fixed using 4% paraformaldehyde solution for 15 min. A solution of Triton X-100 at 0.1% was added for 15 min to permeabilize cells. A solution of 5% BSA was used for 30 min to block unspecific interaction sites. Then, cells were incubated with antibody solutions of anti-EEA-1-AF488 (10 μg/mL) or anti-Lamp1-AF488 (1.25 μg/mL) antibodies in 1% BSA for 30 min and then washed with DPBS 1×. The staining of the cell

DOI: 10.1021/acs.biomac.9b00637
Biomacromolecules 2019, 20, 3076−3086

membrane with WGA-AF488 was done as described in Section 2.7.2. After the staining, cells were mounted with Fluoromount-G. Cells were visualized and imaged with a confocal microscope Nikon A1R using ×60/1.4 objective and NIS elements software. Images were acquired with a resolution of 0.21 μm/px and were constructed using Fiji software (ImageJ).

2.9.2. Imaging Flow Cytometry (Amnis ImageStream^X Mark II). MDA-MB-231 cells were seeded at 2 × 10^6 cells per well in a 6-well plate for 24 h. After cellular adhesion, cells were incubated with CS-MSN or S-MSN prepared with the siRNA-Atto390 conjugate (50 nM siRNA). The fluorescence of the siRNA-Atto390 conjugate and sulfocyanine 5 conjugated to CS-FNP or S-FNP was monitored in early endosomes and lysosomes after incubation with CS-MSN or S-MSN, respectively. MDA-MB-231 cells were incubated with CS-MSN or S-MSN prepared with the siRNA-Atto390 conjugate for 4 h, then the cell culture medium was changed, and cells were incubated or not for additional 20 h. After that, cells were stained with anti-EEA-1-AF488 (channel 2) or anti-Lamp1-AF488 (channel 2) antibodies as described in Section 2.8.1. In each experiment, 10 000 events for each sample were acquired with Inspire imaging flow cytometry software using Amnis ImageStream^X Mark II. MDA-MB-231 images were captured at 60× magnification and EDF. Single-stained samples of 500 cells were also illuminated by the 405 nm (70 mW), 488 nm (100 mW), and 642 nm (150 mW) lasers with the brightfield (BF) and darkfield inactivated to perform color compensation controls. The spectral compensation matrix was applied to each of the files. Cells in the best focus were identified using Gradient RMS of the BF image. Single cells were then separated from debris and doublets using a plot of the aspect ratio vs the area of the BF image. The internalization scores (IS) of siRNA-Atto390 (channel 7) and that of sulfocyanine 5 (channel 11) conjugated to CS-FNP or S-FNP were analyzed in early endosome and lysosomes using "fluorescent intracellular compartment mask" [Erode (M02, 4)] and calculated using the internalization feature provided by IDEAS V6.2 software.

2.9.3. Structured Illumination Microscopy (SIM). Cells were prepared and stained with anti-EEA-1-Alexa Fluor 488 antibody as described in Section 2.8.1. After that, cells were analyzed and imaged with a structured illumination microscope Nikon N-SIM using ×100/1.49 objective and NIS elements software. Images were acquired with a resolution of 0.03 μm/px and were constructed by Fiji software.

2.9.4. Downregulation of GFP Protein and Inhibition of Endosomal Acidification. After 24 h of the seeding of MDA-MB-231/GFP (Euromedex, Souffelweyersheim, France) at 30 × 10^3 cells per well in a 12-well plate, cells were pretreated or not for 1 h with an inhibitor of endosomal acidification, bafilomycin A1 (5 μM, Enzo Life Science, Villeurbanne, France), then a transfection assay was carried out as described in our previous publication.[18] Briefly, S-MSN and CS-MSN were prepared according to the formulation protocol with anti-GFP siRNA. S-MSN or CS-MSN formulation (50 nM siRNA) was added to cells after replacement of the complete cell culture medium by the transfection medium. After 4 h, the transfection medium was replaced with the complete cell culture medium and then cells were incubated in normal growth conditions until 72 h. Nontreated cells were used as a negative control, and cells treated with the commercial transfection agent Oligofectamine (Invitrogen, Thermo Fisher Scientific, Paisley, U.K.) were used as a positive control (cells were transfected with Oligofectamine according to the manufacturer's recommendations). Cells were removed using 0.05% trypsin−EDTA, gene silencing was evaluated using Gallios flow cytometry, and data were analyzed by FlowJo v10 software.

2.10. Statistics. PRISM (GraphPad Prism 7) was used for statistical analysis. Data were compared among groups using the Mann−Whitney test. The difference between groups was considered significant when p-value <0.05 (*) or <0.01 (**). # is the reference value for statistics.

3. RESULTS AND DISCUSSION

3.1. Nanoparticle Characterizations. To eliminate the nongrafted gH625 peptide, suspensions of CS-FNP and the control S-FNP were purified by size-exclusion chromatography (SEC). The SEC chromatogram of S-FNP showed only one peak, which corresponds to the absorbance of SPION (Figure 1A). However, the SEC chromatogram of CS-FNP showed

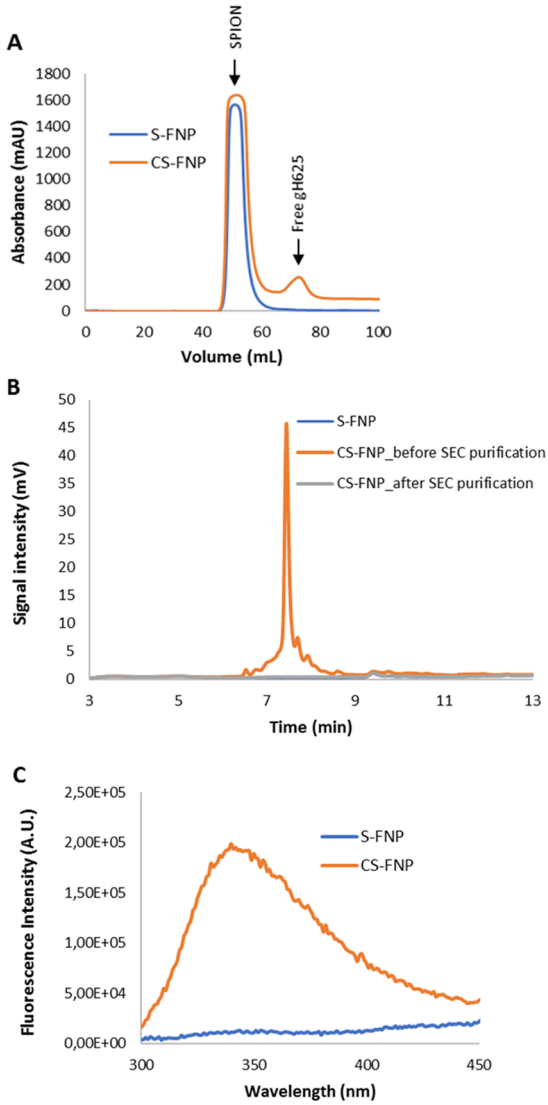

Figure 1. (A) Chromatograms of the purification of S-FNP and CS-FNP by SEC. (B) HPLC chromatograms of S-FNP and CS-FNP before and after SEC purification for the detection of free gH625. (C) Fluorescence profiles of the tryptophan-based gH625 peptide in S-FNP and CS-FNP after excitation at 280 nm.

two peaks. According to their respective sizes, the first one corresponds to SPION (at 50 mL) and the second one corresponds to the free gH625 peptide (at 75 mL). Thereafter, high-performance liquid chromatography (HPLC) was used to check and quantify the presence of the free peptide in purified CS-FNP suspensions and to determine the grafting efficiency on nanoparticles. Only free gH625 is detected with this technique as an identifiable peak (Figure S1). Therefore, HPLC was used to check and quantify the fractions of the free gH625 peptide collected from SEC purification. The chromatograms show that no gH625 peak was observed in purified CS-FNP contrary to nonpurified CS-FNP (Figure 1B). This indicates that SEC is an efficient method to eliminate nongrafted peptides. The amount of the free peptide collected

DOI: 10.1021/acs.biomac.9b00637
Biomacromolecules 2019, 20, 3076−3086

from SEC purification represented 9.75 ± 1.38% of the total amount of peptides used for the grafting. Subsequently, the presence of the gH625 peptide grafted on nanoparticles was assessed by detecting the fluorescence of its tryptophan residue. The presence of gH625 on the surface of CS-FNP was confirmed by the strong fluorescence signal of tryptophan under excitation at 280 nm and with a maximum emission at 340 nm (Figure 1C). Control nanoparticles (S-FNP) showed no fluorescence at 340 nm because of the absence of peptides.

The physicochemical properties of synthesized nanoparticles with or without gH625 were then determined. The hydrodynamic diameters (HD) were 73 ± 6 and 86 ± 6 nm, respectively, for S-FNP and CS-FNP with a polydispersity index below 0.2 (Table 1 and Figure S2). No significant difference between the ζ-potential of S-FNP and CS-FNP was observed. Therefore, the presence of gH625 at the surface of our nanoparticles did not perturb their physicochemical properties, no significant increase of the HD was observed, and the surface of SPION remained almost neutral. Taking all of these results together, we successfully grafted the gH625 peptide at the surface of PEGylated SPION at a grafting efficiency of almost 90% and with suitable colloidal properties for injectable nanoformulations.

Table 1. Hydrodynamic Diameter (HD), Polydispersity Index (PDI), and ζ-Potential (ZP) of S-FNP and CS-FNP

	HD (nm)	PDI	ZP (mV)
S-FNP	73 ± 6	0.19 ± 0.05	−6 ± 1
CS-FNP	86 ± 6	0.18 ± 0.02	−7 ± 2

3.2. Formulation and Characterization of siRNA Nanovectors. Subsequently, S-FNP and CS-FNP were used as a nanoplatform for the formulation of siRNA delivery nanovectors called S-MSN and CS-MSN denoting stealth magnetic siRNA nanovector and CPP-capped stealth magnetic siRNA nanovector, respectively (Figure 2). The formulation of

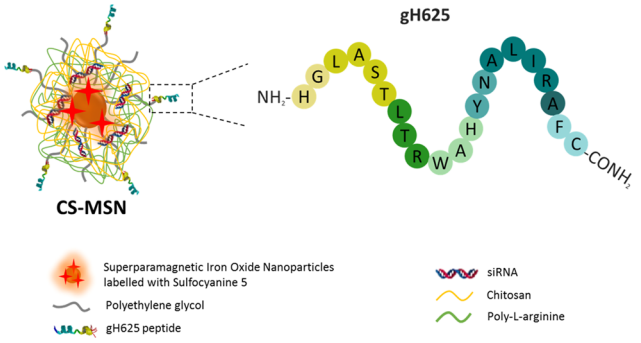

Figure 2. Schematic illustration of CS-MSN with the gH625 peptide sequence.

S-MSN and CS-MSN was performed according to our previously optimized protocol.[18] The size values of S-MSN and CS-MSN were 155 and 150 nm, respectively, with a polydispersity index of almost 0.3. The ζ-potentials of S-MSN (+16 mV) and CS-MSN (+13 mV) were slightly positive thanks to the presence of cationic polymers (Table 2 and Figure S3). These results showed that no significant differences were observed in the physicochemical characteristics of the nanovectors formulated with S-FNP and CS-FNP. Moreover, the loading of siRNA in S-MSN and CS-MSN was checked

Table 2. Hydrodynamic Diameter (HD), Polydispersity Index (PDI), and ζ-Potential (ZP) of S-MSN and CS-MSN

	HD (nm)	PDI	ZP (mV)
S-MSN	155 ± 15	0.30 ± 0.05	+16 ± 2
CS-MSN	150 ± 13	0.29 ± 0.04	+13 ± 1

using a gel retardation assay. As shown in Figure 3, no fluorescence was detected in the case of S-MSN and CS-MSN.

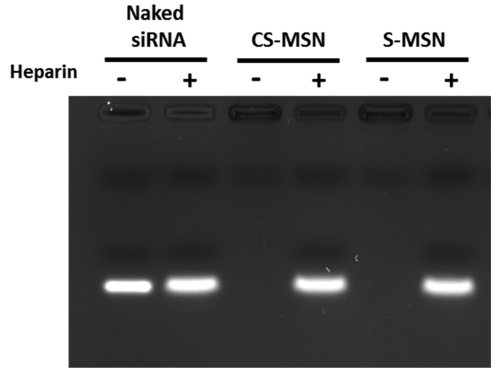

Figure 3. Gel retardation assay to detect free siRNA in S-MSN and CS-MSN.

However, in the presence of heparin, fluorescent bands appear at the same fluorescence intensity as the control free siRNA. This result showed that siRNA are completely complexed in both nanovectors, as it was shown for CS-MSN in our previously published results.[18] Therefore, the presence of the peptide gH625 did not affect the complexation of siRNA with cationic polymers and with the nanoplatforms (S-FNP and CS-FNP).

3.3. Internalization Mechanisms and Intracellular Trafficking of siRNA Nanovectors. *3.3.1. Cell Uptake.* The internalization of CS-MSN and S-MSN in cells was investigated using confocal microscopy by detecting the fluorescence of the sulfocyanine 5-labeled (C)S-FNP or siRNA-Atto390 conjugate at a concentration of 50 nM (siRNA equivalent). The labeling of the cell membrane appears in green in images. The fluorescence related to nanovectors [pink or red spots corresponding to (C)S-MSN or (C)S-FNP] was found inside the cell, showing that nanovectors were internalized by the cells and were more abundant in the condition CS-MSN, i.e., when the siRNA nanovectors were functionalized with the CPP gH625 (Figure 4).

The uptake kinetics of siRNA nanovectors (S-MSN and CS-MSN) in triple-negative breast cancer cells was performed up to 4 h by monitoring the fluorescence of the sulfocyanine 5-labeled (C)S-FNP or siRNA-Atto390 conjugate. As shown in Figure 5A, the fluorescence intensity of sulfocyanine increased up to 4 h for both nanovectors, CS-MSN and S-MSN (Figure 5B). The presence of the peptide gH625 enhances the entry of CS-MSN in cells starting from 2 h compared to S-MSN, and this entry is approximately 2.5-fold higher for CS-MSN after 4 h of incubation. The same kind of results was found when monitoring the fluorescence of Atto390 conjugated to siRNA (Figure S4).

The potential of CPP to enhance the internalization of conjugated nanovectors has already been demonstrated,[19−21] as well as that of gH625 peptide.[10,11] In a previous study, we demonstrated an increase of the cell uptake of doxorubicin-

DOI: 10.1021/acs.biomac.9b00637
Biomacromolecules 2019, 20, 3076−3086

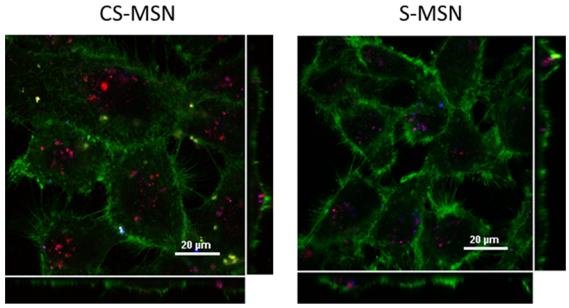

Figure 4. Confocal images of MDA-MB-231 cells treated with CS-MSN (left image) or S-MSN (right image) for 4 h and stained with wheat germ agglutinin-Alexa Fluor 488 as a membrane stain (green). Red fluorescence: Sulfocyanine 5 conjugated to CS-FNP or S-FNP; blue fluorescence: Atto390 conjugated to siRNA. The scale bar is 20 μm.

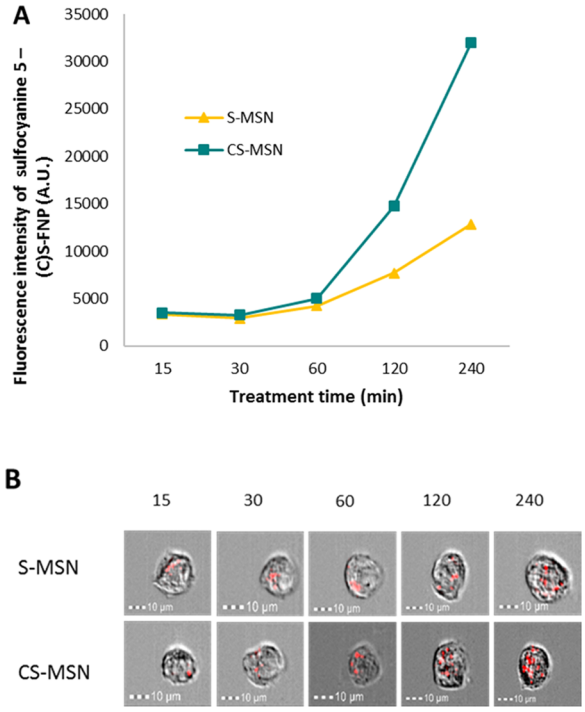

Figure 5. Uptake kinetics of CS-MSN and S-MSN in MDA-MB-231 cells. Intracellular fluorescence intensity of sulfocyanine 5 conjugated to CS-FNP or S-FNP was monitored by imaging flow cytometry after the incubation of nanovectors for 15, 30, 60, 120, and 240 min: (A) intracellular fluorescence intensity and (B) representative brightfield images of cells containing intracellular fluorescent nanovectors (red spots) derived from the imaging flow cytometry data collection.

loaded liposomes by conjugating the peptide gH625 on the surface of the liposomes.[10] In another study, Valiante and co-workers showed the success of the peptide gH625 to cross an *in vitro* model of the blood–brain barrier and the ability to deliver a conjugated cargo into neuron and astrocyte cells.[11] The enhanced internalization of the nanovectors in the presence of gH625 can be supported by the presence of both hydrophobic and hydrophilic amino acids in the sequence of this CPP.[22] The correct balance of this characteristic enables the local and temporary destabilization of the membrane bilayer favoring a direct crossing of the membrane. Apart from the presence of both hydrophobic and hydrophilic residues, several other structural features are responsible for the gH625 cell internalization mechanism such as the ability to change from a random to an amphipathic α-helical structure when in contact with membrane bilayers, the ability to oligomerize in membrane bilayers, and the presence of a histidine residue at the N-terminus.[23] In the present study, the increase of the cell internalization of CS-MSN by gH625 shows that this nanovector may be an efficient system for the delivery of siRNA in cancer cells.

3.3.2. Internalization Pathway. The pathway used to enter cells could determine the intracellular trafficking of nanovectors and affects their efficiency to deliver their contents. To determine the internalization pathway of S-MSN and CS-MSN, the fluorescence intensity of sulfocyanine 5 conjugated to S-FNP or CS-FNP was measured after incubation with chemical inhibitors. As shown in Figure 6A, the incubation of cells with the combination of sodium azide and 2-deoxy-D-glucose (energy inhibitors) or with dynasore (dynamin inhibitor) resulted in an evident reduction of the sulfocyanine 5 fluorescence intensity in treated cells. Indeed, in the cells pretreated with energy inhibitors, the fluorescence intensity decreased from 100 to 26 ± 11 and 24 ± 16% for S-MSN and CS-MSN, respectively, and to 30 ± 7 and 33 ± 7% in cells incubated with dynasore. These decreases in fluorescence intensity indicate a reduction of S-MSN and CS-MSN cell uptake and therefore an inhibition of nanovector internalization by the cells. Nevertheless, there is no significant difference between the two kinds of nanovectors. This result implies that the entry of S-MSN and CS-MSN was energy- and dynamin-dependent; thus, the internalization process may be an endocytosis phenomenon. Moreover, the analysis of MDA-MB-231 cells treated with the nanovectors and stained with the membrane marker (WGA-AF488), by confocal microscopy, shows highly fluorescent intracellular spots (Figure 6B) representing the colocalization of fluorophores conjugated to nanovectors (sulfocyanine 5 and Atto390) and fluorophore conjugated to the membrane marker (AF488). These bright spots look like vesicles formed from the cell membrane, as they were stained with Alexa Fluor 488 conjugated to WGA, containing nanovectors (Figure 6B, white arrows), such as endosomes. This result confirms the hypothesis of an endocytic pathway for the internalization route of (C)S-MSN into MDA-MB-231 cells. In addition, to specify the used endocytic pathway, we evaluated the internalization of nanovectors in the presence of some chemical inhibitors of endocytic pathways. Figure 6B shows a significant reduction of the intracellular fluorescence intensity of both nanovectors after incubation for cells with caveolae-mediated endocytosis inhibitors, methyl-β-cyclodextrin (MβCD) and nystatin. The effect of pitstop 2, a clathrin inhibitor, in the internalization of S-MSN and CS-MSN was investigated, and results show a significant decrease of cell uptake. In contrast, no effect was observed after the cell incubation with chlorpromazine, a clathrin inhibitor, and dimethyl amiloride (DMA), an inhibitor of macropinocytosis. Thus, one concludes that the internalization occurs via endocytosis mediated by clathrin and caveolae.

Furthermore, MDA-MB-231 cells were analyzed by transmission electron microscopy (TEM) after their incubation with S-MSN or CS-MSN to visualize their localization in the cells. TEM images showed the presence of nanovectors in clathrin-coated and caveolae vesicles (Figure 6D). Thus, these images confirmed the endocytic mechanism and the internalization of S-MSN and CS-MSN via both clathrin- and

DOI: 10.1021/acs.biomac.9b00637
Biomacromolecules 2019, 20, 3076–3086

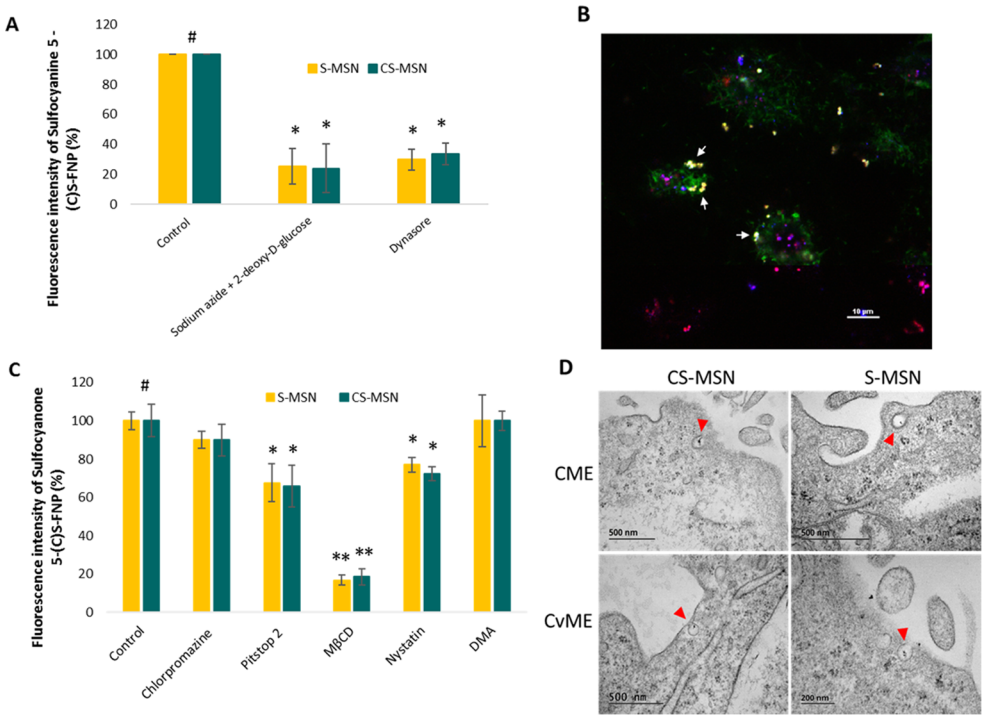

Figure 6. Mechanism and pathway of entry of the siRNA nanovectors: (A) Fluorescence intensity of sulfocyanine 5 conjugated to S-FNP or CS-FNP measured by flow cytometry in MDA-MB-231 cells incubated with nanovectors with or without sodium azide and 2-deoxy-D-glucose or dynasore. (B) Confocal microscopy image of MDA-MB-231 cells treated with CS-MSN for 4 h and stained with WGA-AF488. (C) Fluorescence intensity of sulfocyanine 5 conjugated to S-FNP or CS-FNP measured by flow cytometry in MDA-MB-231 cells incubated with nanovectors with or without chlorpromazine, methyl-β-cyclodextrin (MβCD), pitstop 2, nystatin, or dimethyl amiloride (DMA). (D) Transmission electron microscopy images of MDA-MB-231 cells incubated with S-MSN or CS-MSN for 4 h. The scale bar is 500 nm.

caveolae-dependent endocytosis pathways. From these results, we showed that the presence of gH625 was able to enhance the internalization (Figure 5) but did not affect the entry route of our siRNA nanovectors. We can, therefore, conclude that even if gH625 is known for its ability to translocate directly into the cytosol, the CPP-conjugated nanovectors follow an endocytic pathway. Without polyplex loading, nanoparticles CS-FNP have been shown to be endocytosed by MDA-MB-231 cells.[17] In their study, Carberry et al. showed that the functionalization of a dendrimer with the peptide gH625 leads to cell internalization involving both direct translocation and endocytosis.[9] In the same context, Madani et al. reported, in their review, that the conjugated cargo could modify the internalization pathway of the CPP.[24] In the present study, we demonstrated that the presence of gH625 at the surface of the nanovector did not modify the entry pathway of CS-MSN and that siRNA nanovectors were internalized by both clathrin- and caveolae-mediated endocytosis.

3.3.3. Intracellular Trafficking of siRNA Nanovectors. The intracellular trafficking of siRNA nanovectors was investigated using intracellular compartments markers. Therefore, cells were incubated with S-MSN or CS-MSN, then stained with an anti-EEA-1 antibody as an early endosome marker (Figure 7A) or an anti-Lamp1 antibody to label the lysosomes of the cells (Figure 7B). Images of cells treated with the siRNA nanovectors after endosomal staining show both nanovector fluorophores [sulfocyanine 5 conjugated to (C)S-FNP (red) and Atto390 conjugated to siRNA (blue)] inside green vesicles (AF488 conjugated to the endosomal marker) at 4 h (Figure 7A). Therefore, these images indicate the presence of S-MSN and CS-MSN in early endosomes after 4 h of incubation. However, after 24 h of incubation, the colocalization of nanovector dyes and fluorophore conjugated to EEA-1 antibody seems to be reduced as we can observe more red spots alone (Figure 7A). That indicates either a progression toward lysosomes or the escape of nanovectors from endosomes. Moreover, images of cells treated with nanovectors after lysosomal staining show at 4 h a low colocalization of sulfocyanine 5 (red) and Atto390 (blue) nanovector fluorophores with AF488 conjugated to the lysosomal marker (green) (Figure 7B). This colocalization increased after 24 h mainly with sulfocyanine 5 (red) conjugated to nanoparticles (S-FNP and CS-FNP). That indicates that the accumulation of nanoparticles in lysosomes was higher than that of siRNA.

To confirm this tendency, treated cells were also analyzed by imaging flow cytometry and the internalization scores (IS) of sulfocyanine 5 and Atto390 in endosomes or lysosomes were determined (Table 3). The IS measure the relative amount of a signal inside versus outside endosomes or lysosomes. The higher the score, the greater the quantity of nanovectors found in the organelle. In this study, we especially investigated the variation of the IS between 4 and 24 h in early endosomes and lysosomes for the nanovectors with or without gH625. For S-MSN, the internalization scores of siRNA and S-FNP in early endosomes largely increased after 24 h compared to 4 h, which indicates an accumulation of S-MSN in early endosomes (0.4 vs 1.3 and 0.5 vs 1.6, respectively). On the contrary, the internalization scores of siRNA and CS-FNP of CS-MSN in early endosomes did not change so much (0.6 vs 0.5 and 0.4 vs 0.7, respectively). This result suggests that the presence of the gH625 peptide in the nanovector promotes the endosomal escape. In lysosomes, the internalization score of nanovector

DOI: 10.1021/acs.biomac.9b00637
Biomacromolecules 2019, 20, 3076−3086

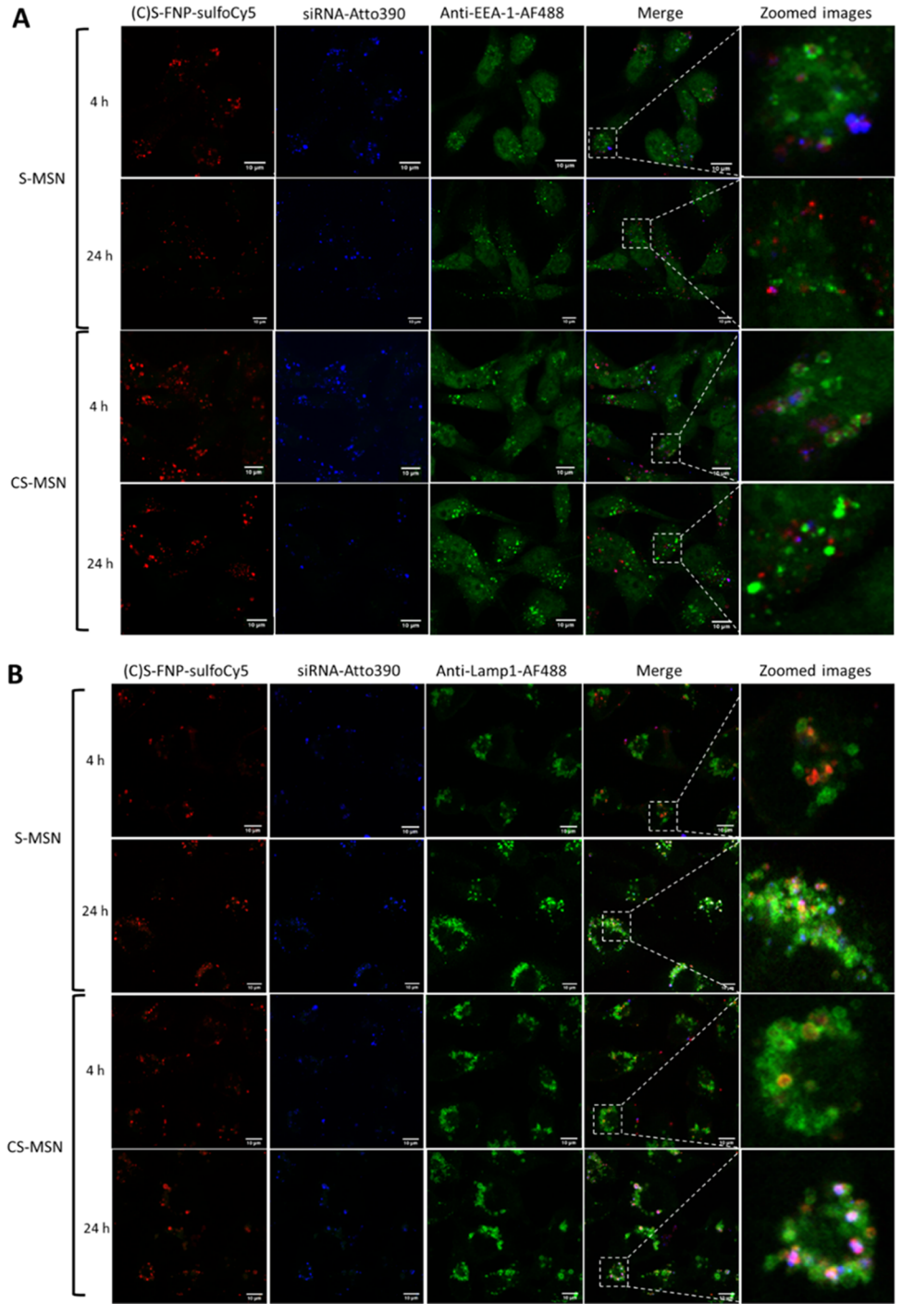

Figure 7. Intracellular trafficking of S-MSN and CS-MSN in MDA-MB-231 cells. Colocalization of siRNA-Atto390 (blue) and CS-FNP or S-FNP conjugated with sulfocyanine 5 (red) with (A) anti-EEA-1-AF480 antibody and (B) anti-Lamp1-AF488 antibody (green) after 4 h of contact. The staining and cell fixation were made immediately (4 h) or 20 h later (24 h), followed by confocal imaging.

Table 3. Variation of the Internalization Score (IS) between 4 and 24 h of siRNA or (C)S-FNP of S-MSN or CS-MSN in Early Endosomes and in Lysosomes

	early endosomes (anti-EEA-1 antibody)				lysosomes (anti-Lamp1 antibody)			
	siRNA		(C)S-FNP		siRNA		(C)S-FNP	
incubation time	4 h	24 h	4 h	24 h	4 h	24 h	4 h	24 h
S-MSN	0.4	1.3	0.5	1.6	1.1	1.3	0.6	1.7
CS-MSN	0.6	0.5	0.4	0.7	1.2	1.5	0.7	1.7

DOI: 10.1021/acs.biomac.9b00637
Biomacromolecules 2019, 20, 3076−3086

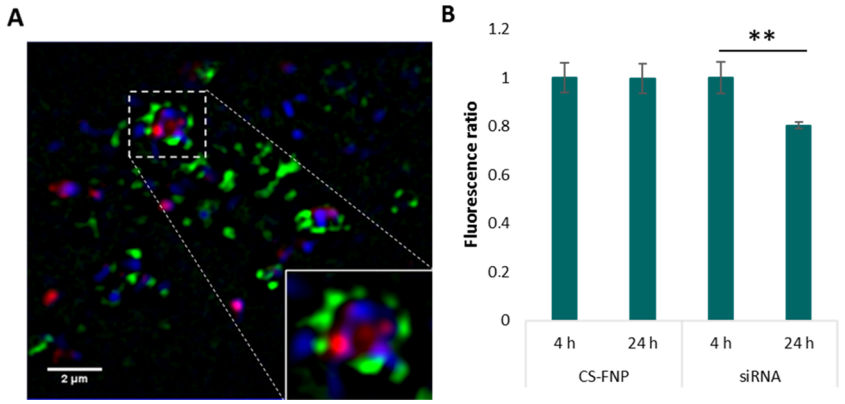

Figure 8. Endosomal escape of nanovectorized siRNA with CS-MSN. (A) Structured illumination microscopy (SIM) image of MDA-MB-231 cells incubated with CS-MSN prepared with siRNA-Atto390 and anti-EEA-1-AF488 antibody. The scale bar is 2 μm. (B) Ratio of the fluorescence intensity of sulfocyanine 5 and Atto390 conjugated to CS-FNP and siRNA, respectively, in cells treated with CS-MSN for 4 h or 24 h measured by flow cytometry.

cores (S-FNP and CS-FNP) increased strongly, showing progressive accumulation in lysosomes. However, the internalization score of siRNA of both nanovectors (S-MSN and CS-MSN) did not increase significantly. This could suggest that siRNA were freed before reaching the lysosomes.

In this part of the study, some discrepancies between confocal microscopy and imaging flow cytometry results were observed. For example, in the case of S-MSN, the increase of the internalization score of siRNA or S-FNP in early endosomes after 24 h was not detected in confocal microscopy. On the contrary, a reduction of the colocalization of the fluorescence of Atto390 or sulfocyanine 5 conjugated to siRNA or S-FNP, respectively, and that of AF488 conjugated to the endosomal marker was observed. This discrepancy could be explained by a hypothesis reported by Selby and co-workers in their review. With the presence of endosomal and lysosomal markers in the vesicular membrane, an enclosed part of the nanovectors can be missed.[25] Indeed, the analysis of the cells with confocal microscopy can illustrate this limitation as it is based on the fluorescence colocalization. However, the calculation of the IS in intracellular compartments considers even enclosed nanovectors. Therefore, the analysis of the colocalization in images and the internalization score were complementary.

Results of the intracellular trafficking suggest an escape of siRNA from endosomes, which is enhanced by the presence of the peptide gH625, whereas nanoparticles (S-FNP and CS-FNP) continue their trafficking into lysosomes. However, this traffic is possible only if endosomes are not destroyed. Previous studies reported that, in the presence of cationic polymers, the complete rupture of the endosomal membrane is highly unlikely.[26−28] One hypothesis is that the endosomal escape occurs by local endosomal membrane destabilization provoked by the increase of the positive charge density of the cationic polymers. This destabilization results in the permeabilization of the membrane and the formation of transient "nanoscale holes".[29] Thus, to complete this study and to verify this hypothesis, the investigation of the endosomal escape of CS-MSN is needed.

3.3.4. Endosomal Escape of siRNA and Down-regulation Efficiency of CS-MSN. To achieve their mission, nanovectorized siRNA need to be released from the nanovectors and must be found in the cytosol. For that, the endosomal escape represents a major step for siRNA delivery. To investigate the capability of siRNA loaded in CS-MSN to escape endosomes, MDA-MB-231 cells incubated with nanovectors prepared with fluorescent siRNA (siRNA-Atto390) and stained with conjugated anti-EEA-1 antibody were imaged using structured illumination microscopy (SIM) and the intensity of CS-MSN's fluorophores, conjugated to siRNA and CS-FNP, was measured by imaging flow cytometry.

SIM images show the breaking of endosomes (green) and the escape of siRNA (blue) in the cytosol (Figure 8A). The measurement of the fluorescence intensity of the fluorophores conjugated to siRNA (Atto390) and CS-FNP (sulfocyanine 5) in cells treated with CS-MSN for 4 and 24 h shows a significant decrease of the fluorescence intensity of Atto390 conjugated to siRNA after 24 h compared to 4 h, whereas that of sulfocyanine 5 conjugated to CS-FNP remained constant (Figure 8B). The reduction of the siRNA fluorescence intensity could be explained by the dispersion of siRNA in the cytosol, which suggests (1) the endosomal escape of siRNA or (2) their degradation. To invalidate the second hypothesis, a downregulation experiment was performed on MDA-MB-231/GFP cells.

Cells were alternatively treated with the commercial transfection agent Oligofectamine, with S-MSN or CS-MSN formulated with an anti-GFP siRNA for 4 h, and the fluorescence intensity of GFP was measured using flow cytometry after 72 h of the treatment. As shown in Figure 9, the cell GFP expression was reduced using both siRNA nanovectors. This could be explained by the ability of cationic polymers (chitosan and poly-L-arginine) to deliver siRNA in cells.[30,31] Furthermore, the efficiency of CS-MSN to inhibit the GFP in cells was 1.7-fold higher than that of S-MSN. This difference of transfection efficiency for the nanovectors with and without the CPP gH625 could be explained by the increased internalization of CS-MSN and by the enhanced endosomal escape in the presence of gH625. In the literature, many virus-derived peptides are known for their ability to escape endosomes and were used as endosomal escape agents or to enhance the endosomal escape of some molecules. These peptides use various mechanisms to pass through the endosomal membrane such as membrane fusion, pore formation, and proton sponge mechanisms. Oliveira and colleagues used a lipid-based nanovector with influenza-derived peptide diINF-7 for siRNA delivery to silence the epidermal growth factor receptor and the K-ras oncogenes.

DOI: 10.1021/acs.biomac.9b00637
Biomacromolecules 2019, 20, 3076−3086

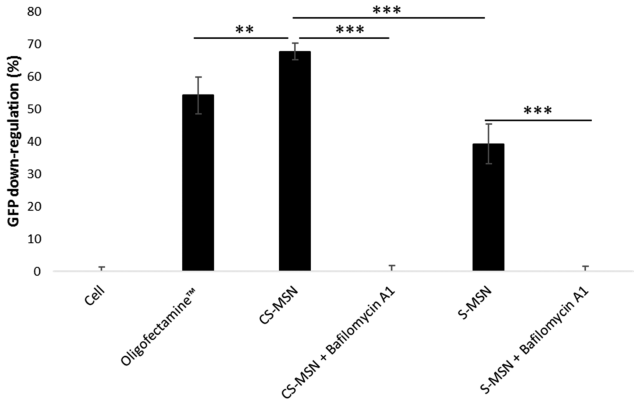

Figure 9. Quantification of GFP downregulation efficiency in MDA-MB-231/GFP cells pretreated or not with bafilomycin A1 and treated with Oligofectamine, CS-MSN, or S-MSN for 4 h and analyzed after 72 h of the treatment using flow cytometry.

The presence of this peptide efficiently enhances the endosomal escape of this complex.[32] This peptide is known to be able to fuse with the membrane of endosomes to facilitate the passage of associated cargo toward the cytosol.[33] For gH625, the mechanism of endosomal escape is not well understood, but based on our SIM results (Figure 8A), the hypothesis of transient pore formation in the endosomal membrane is highly likely. This hypothesis was supported by results presented by Guarnieri et al. where they showed that nanoparticles decorated on their surface with gH625 were able to escape the endo/lysosomal compartment by local and temporary destabilization of the membrane.[34] This ability of the gH625 peptide to escape endosomes results in improving the delivery of therapeutics, which was confirmed in the literature by Galdiero's team using different delivery systems.[22] For example, the conjugation of this peptide to liposomes enhanced the delivery of loaded doxorubicin in doxorubicin-resistant A549 cells and results in an induction of cell death, significantly more pronounced than liposomes without gH625 or free doxorubicin.[10]

Moreover, the pretreatment of cells with an inhibitor of endosomal acidification, bafilomycin A1, blocked the inhibition of the GFP fluorescence and reduced the transfection efficiency of both nanovectors with and without gH625. This result could be explained by the dependence of the endosomal escape mechanism on the acidification of this compartment. In fact, the inhibition of the acidification of endosomes affects the mechanisms of the proton sponge effect and the umbrella effect and blocks the transfer of siRNA to the cytosol. Furthermore, in a previous study, we proved that in a solution of trifluoroethanol, that mimics the environment of cellular membranes, the CPP gH625 changes its conformation to α-helix, which favors the membranotropic properties of this peptide.[17] However, by blocking the umbrella effect of polymers, the contact between the peptide gH625 and the cell membrane can be reduced. Thus, the inhibition of the acidification of endosomes preserved the integrity of the endosomal membrane and prevented the endosomal escape.

4. CONCLUSIONS

In this study, we highlighted the role of a cell-penetrating peptide gH625 in the internalization and the intracellular trafficking of siRNA magnetic nanovectors (CS-MSN). We showed that the cellular uptake of CS-MSN was increased 2.5-fold in the presence of gH625 in a triple-negative breast cancer cell line. Moreover, this peptide appears to play a major role in the endosomal escape. In fact, the functionalization of our siRNA nanovectors with this peptide enhances their passage into the cytosol. In addition to the induction of the endosomal escape with cationic polymers, we suggested that the peptide gH625 may interact with the endosomal membrane and probably promotes transient pore formation, which enhances the escape of siRNA from endosomes. The enhanced entry and the endosomal escape offered by CS-MSN result in high transfection efficiency, 1.7-fold higher than the same nanovector without gH625 peptide.

■ ASSOCIATED CONTENT

Supporting Information

The Supporting Information is available free of charge on the ACS Publications website at DOI: 10.1021/acs.biomac.9b00637.

HPLC chromatograms and a calibration curve of gH625 solutions (Figure S1); size distribution profiles of S-FNP and CS-FNP (Figure S2); size distribution profiles of S-MSN and CS-MSN (Figure S3); uptake kinetics of nanovectorized siRNA obtained by flow imaging (Figure S4) (PDF)

■ AUTHOR INFORMATION

Corresponding Author

*E-mail: emilie.allard@univ-tours.fr.

ORCID

Katel Hervé-Aubert: 0000-0002-3315-903X

Martin Soucé: 0000-0002-6627-9660

Emilie Allard-Vannier: 0000-0002-6973-6812

Funding

We are grateful to the "Ligue Nationale Contre le Cancer" for their financial support and especially to the local committees of the departments 17, 37, 49, 53, and 56 (EVASION project and INTERACTION project). We also thank the "Région Centre-Val de Loire", the "Cancéropole Grand Ouest" (MATURE project), and Campus France (PHC GALILEE 2017, project No 39635TB) for the funding.

Notes

The authors declare no competing financial interest.

■ ACKNOWLEDGMENTS

We thank Nicolas Aubrey (UMR INRA 1282, team of "Infectiologie et Santé Publique", University of Tours) for his help in SEC experiments. We are grateful to Julien Burlaud-Gaillard (Département des Microscopies, Université de Tours, France) for TEM images. Our data were obtained with the assistance of the IBiSA Electron Microscopy Facility of Tours University. The authors would like to thank Thibaut Blondy (CRCINA, Inserm U1232, team 4, University of Nantes) for his help with confocal microscopy experiments.

■ REFERENCES

(1) Tokatlian, T.; Segura, T. siRNA Applications in Nanomedicine. *Wiley Interdiscip. Rev.: Nanomed. Nanobiotechnol.* **2010**, 305−315.

(2) Videira, M.; Arranja, A.; Rafael, D.; Gaspar, R. Preclinical Development of SiRNA Therapeutics: Towards the Match between Fundamental Science and Engineered Systems. *Nanomedicine* **2014**, *10*, 689−702.

DOI: 10.1021/acs.biomac.9b00637
Biomacromolecules 2019, 20, 3076−3086

(3) Wang, J.; Lu, Z.; Wientjes, M. G.; Au, J. L.-S. Delivery of SiRNA Therapeutics: Barriers and Carriers. *AAPS J.* **2010**, *12*, 492−503.
(4) Steinbach, J. M.; Seo, Y.-E.; Saltzman, W. M. Cell Penetrating Peptide-Modified Poly(Lactic-Co-Glycolic Acid) Nanoparticles with Enhanced Cell Internalization. *Acta Biomater.* **2016**, *30*, 49−61.
(5) Guan, X.; Hu, X.; Cui, F.; Li, Y.; Jing, X.; Xie, Z. EGFP-Based Protein Nanoparticles with Cell-Penetrating Peptide for Efficient SiRNA Delivery. *Macromol. Biosci.* **2015**, *15*, 1484−1489.
(6) Malhotra, M.; Tomaro-Duchesneau, C.; Prakash, S. Synthesis of TAT Peptide-Tagged PEGylated Chitosan Nanoparticles for SiRNA Delivery Targeting Neurodegenerative Diseases. *Biomaterials* **2013**, *34*, 1270−1280.
(7) Gräslund, A.; Madani, F.; Lindberg, S.; Langel, Ü.; Futaki, S.; Gräslund, A.; Madani, F.; Lindberg, S.; Langel, Ü.; Futaki, S. Mechanisms of Cellular Uptake of Cell-Penetrating Peptides. *J. Biophys.* **2011**, *2011*, No. 414729.
(8) Galdiero, S.; Falanga, A.; Morelli, G.; Galdiero, M. GH625: A Milestone in Understanding the Many Roles of Membranotropic Peptides. *Biochim. Biophys. Acta, Biomembr.* **2015**, *1848*, 16−25.
(9) Carberry, T. P.; Tarallo, R.; Falanga, A.; Finamore, E.; Galdiero, M.; Weck, M.; Galdiero, S. Dendrimer Functionalization with a Membrane-Interacting Domain of Herpes Simplex Virus Type 1: Towards Intracellular Delivery. *Chem. - Eur. J.* **2012**, *18*, 13678−13685.
(10) Perillo, E.; Porto, S.; Falanga, A.; Zappavigna, S.; Stiuso, P.; Tirino, V.; Desiderio, V.; Papaccio, G.; Galdiero, M.; Giordano, A.; Galdiero, S.; Caraglia, M. Liposome Armed with Herpes Virus-Derived GH625 Peptide to Overcome Doxorubicin Resistance in Lung Adenocarcinoma Cell Lines. *Oncotarget* **2016**, *7*, 4077−4092.
(11) Valiante, S.; Falanga, A.; Cigliano, L.; Iachetta, G.; Busiello, R. A.; La Marca, V.; Galdiero, M.; Lombardi, A.; Galdiero, S. Peptide GH625 Enters into Neuron and Astrocyte Cell Lines and Crosses the Blood−Brain Barrier in Rats. *Int. J. Nanomed.* **2015**, *10*, 1885−1898.
(12) Falanga, A.; Lombardi, L.; Tarallo, R.; Franci, G.; Perillo, E.; Palomba, L.; Galdiero, M.; Pontoni, D.; Fragneto, G.; Weck, M.; Galdiero, S. The Intriguing Journey of GH625-Dendrimers. *RSC Adv.* **2017**, *7*, 9106−9114.
(13) Venkitaraman, R. Triple-Negative/Basal-like Breast Cancer: Clinical, Pathologic and Molecular Features. *Expert Rev. Anticancer Ther.* **2010**, *10*, 199−207.
(14) Hatakeyama, H.; Akita, H.; Kogure, K.; Oishi, M.; Nagasaki, Y.; Kihira, Y.; Ueno, M.; Kobayashi, H.; Kikuchi, H.; Harashima, H. Development of a Novel Systemic Gene Delivery System for Cancer Therapy with a Tumor-Specific Cleavable PEG-Lipid. *Gene Ther.* **2007**, *14*, 68−77.
(15) Love, K. T.; Mahon, K. P.; Levins, C. G.; Whitehead, K. A.; Querbes, W.; Dorkin, J. R.; Qin, J.; Cantley, W.; Qin, L. L.; Racie, T.; et al. Lipid-like Materials for Low-Dose, in Vivo Gene Silencing. *Proc. Natl. Acad. Sci. U.S.A.* **2010**, *107*, 1864−1869.
(16) Müller, L. K.; Kaps, L.; Schuppan, D.; Brose, A.; Chai, W.; Fischer, K.; Müller, S.; Frey, H.; Schmidt, M.; Mohr, K. Physicochemical and Preclinical Evaluation of Spermine-Derived Surfactant Liposomes for in Vitro and in Vivo SiRNA-Delivery to Liver Macrophages. *Mol. Pharmaceutics* **2016**, *13*, 3636−3647.
(17) Perillo, E.; Hervé-Aubert, K.; Allard-Vannier, E.; Falanga, A.; Galdiero, S.; Chourpa, I. Synthesis and in Vitro Evaluation of Fluorescent and Magnetic Nanoparticles Functionalized with a Cell Penetrating Peptide for Cancer Theranosis. *J. Colloid Interface Sci.* **2017**, *499*, 209−217.
(18) Ben Djemaa, S.; David, S.; Hervé-Aubert, K.; Falanga, A.; Galdiero, S.; Allard-Vannier, E.; Chourpa, I.; Munnier, E. Formulation and in Vitro Evaluation of a SiRNA Delivery Nanosystem Decorated with GH625 Peptide for Triple Negative Breast Cancer Theranosis. *Eur. J. Pharm. Biopharm.* **2018**, *131*, 99−108.
(19) Muratovska, A.; Eccles, M. R. Conjugate for Efficient Delivery of Short Interfering RNA (SiRNA) into Mammalian Cells. *FEBS Lett.* **2004**, *558*, 63−68.
(20) Oh, B.; Lee, M. Combined Delivery of HMGB-1 Box A Peptide and S1PLyase SiRNA in Animal Models of Acute Lung Injury. *J. Controlled Release* **2014**, *175*, 25−35.
(21) Sakurai, Y.; Hatakeyama, H.; Akita, H.; Oishi, M.; Nagasaki, Y.; Futaki, S.; Harashima, H. Efficient Short Interference RNA Delivery to Tumor Cells Using a Combination of Octaarginine, GALA and Tumor-Specific, Cleavable Polyethylene Glycol System. *Biol. Pharm. Bull.* **2009**, *32*, 928−932.
(22) Falanga, A.; Galdiero, M.; Galdiero, S. Membranotropic Cell Penetrating Peptides: The Outstanding Journey. *Int. J. Mol. Sci.* **2015**, *16*, 25323−25337.
(23) Galdiero, S.; Falanga, A.; Vitiello, M.; Raiola, L.; Russo, L.; Pedone, C.; Isernia, C.; Galdiero, M. The Presence of a Single N-Terminal Histidine Residue Enhances the Fusogenic Properties of a Membranotropic Peptide Derived from Herpes Simplex Virus Type 1 Glycoprotein H. *J. Biol. Chem.* **2010**, *285*, 17123−17136.
(24) Tünnemann, G.; Martin, R. M.; Haupt, S.; Patsch, C.; Edenhofer, F.; Cardoso, M. C. Cargo-Dependent Mode of Uptake and Bioavailability of TAT-Containing Proteins and Peptides in Living Cells. *FASEB J.* **2006**, *20*, 1775−1784.
(25) Selby, L. I.; Cortez-Jugo, C. M.; Such, G. K.; Johnston, A. P. R. Nanoescapology: Progress toward Understanding the Endosomal Escape of Polymeric Nanoparticles. *Wiley Interdiscip. Rev.: Nanomed. Nanobiotechnol.* **2017**, *9*, No. e1452.
(26) Trützschler, A. K.; Bus, T.; Reifarth, M.; Brendel, J. C.; Hoeppener, S.; Traeger, A.; Schubert, U. S. Beyond Gene Transfection with Methacrylate-Based Polyplexes - The Influence of the Amino Substitution Pattern. *Bioconjugate Chem.* **2018**, *29*, 2181−2194.
(27) Mishra, S.; Webster, P.; Davis, M. E. PEGylation Significantly Affects Cellular Uptake and Intracellular Trafficking of Non-Viral Gene Delivery Particles. *Eur. J. Cell Biol.* **2004**, *83*, 97−111.
(28) Jonker, C.; de Heus, C.; Faber, L.; ten Brink, C.; Potze, L.; Fermie, J.; Liv, N.; Klumperman, J. An Adapted Protocol to Overcome Endosomal Damage Caused by Polyethylenimine (PEI) Mediated Transfections. *Matters* **2017**, *3*, No. e201711000012.
(29) Schubert, U. S.; Traeger, A.; Bus, T. The Great Escape: How Cationic Polyplexes Overcome the Endosomal Barrier. *J. Mater. Chem. B* **2018**, *6*, 6904−6918.
(30) Xie, Y.; Qiao, H.; Su, Z.; Chen, M.; Ping, Q.; Sun, M. PEGylated Carboxymethyl Chitosan/Calcium Phosphate Hybrid Anionic Nanoparticles Mediated HTERT SiRNA Delivery for Anticancer Therapy. *Biomaterials* **2014**, *35*, 7978−7991.
(31) Veiseh, O.; Kievit, F. M.; Mok, H.; Ayesh, J.; Clark, C.; Fang, C.; Leung, M.; Arami, H.; Park, J. O.; Zhang, M. Cell Transcytosing Poly-Arginine Coated Magnetic Nanovector for Safe and Effective SiRNA Delivery. *Biomaterials* **2011**, *32*, 5717−5725.
(32) Oliveira, S.; van Rooy, I.; Kranenburg, O.; Storm, G.; Schiffelers, R. M. Fusogenic Peptides Enhance Endosomal Escape Improving SiRNA-Induced Silencing of Oncogenes. *Int. J. Pharm.* **2007**, *331*, 211−214.
(33) Varkouhi, A. K.; Scholte, M.; Storm, G.; Haisma, H. J. Endosomal Escape Pathways for Delivery of Biologicals. *J. Controlled Release* **2011**, *151*, 220−228.
(34) Guarnieri, D.; Muscetti, O.; Falanga, A.; Fusco, S.; Belli, V.; Perillo, E.; Battista, E.; Panzetta, V.; Galdiero, S.; Netti, P. A. Surface Decoration with GH625-Membranotropic Peptides as a Method to Escape the Endo-Lysosomal Compartment and Reduce Nanoparticle Toxicity. *Nanotechnology* **2015**, *26*, No. 415101.

DOI: 10.1021/acs.biomac.9b00637
Biomacromolecules 2019, 20, 3076−3086